J Mater Sci (2011) 46:5153–5159
DOI 10.1007/s10853-011-5446-3

Hydrothermal synthesis of silver nanoshells: formation and plasmon hybridization

B. Mondal · S. K. Saha

Received: 21 December 2010 / Accepted: 5 March 2011 / Published online: 22 March 2011

Abstract Silver nanoshells with varying diameters are synthesized using Polyacrylamide (PAM) in a controllable way by the hydrothermal process followed by calcinations to investigate the plasmon hybridization. At relatively lower hydrothermal temperature ($T_H \sim 415$ K), an assembly of silver nanoparticles (NPs) along the PAM chain is formed exhibiting transverse (453 nm) and longitudinal (949 nm) surface plasmon resonance (SPR) peaks. With increasing T_H ($\sim$510 K), this assembly of NPs disrupt into segments and create a homogeneous phase of PAM–silver composites, which upon cooling form globules due to agglomeration. During calcinations at 650 K, PAM is degraded into several gases (NH_3, CO_2, and water vapor) to form nanobubbles, which are trapped inside the globule and coalescence into a single bubble as a result; the molten state containing the NPs forms a spherical shell to minimize the surface energy. The absorption spectra are de-convoluted into three peaks, which are attributed to the hybridization between anti-bonding and bonding SPR modes of individual nanoshells.

Introduction

The optical properties of metal nanostructures have recently attracted a dramatic increase in attention because of their potential applications in fundamentally new nanostructure based optical elements—an emerging area known as "plasmonics" [1–4]. It is well known that the surface plasmon resonance (SPR), which is defined as the collective excitation of conduction electrons, dominates the optical response of metal nanostructures. Usually, frequency of SPR depends on density of the conduction electrons and the geometry of the nanoparticles (NPs). Nanoshells consisting of a spherical dielectric core surrounded by a concentric metal shell, support SPR whose frequencies are determined by inner core and outer shell dimensions. This geometric dependence arises from the hybridization between "cavity plasmons" supported by the inner surface of the shell and the "sphere plasmons" at the outer surface of the shell.

Large volume of theoretical studies have already been done on the interaction of different nanostructures in pairs; like spherical particles [5–9], nanorods [10, 11], nano eggs [1], nanorice [12], and nanoshells [13–16]. So far, a large number of nanostructures such as, nanorods [17, 18], nanorings [19], nanocubes [20], nanoshells [21], and nanodiscs [22] have been synthesized to investigate their optical properties. Nanorods possess two types of SPR modes [23], one longitudinal and the other transverse and these two modes can be tuned by changing the aspect ratio [24]. Theoretical calculations of nanoshells predict two tunable SPR modes one anti-bonding orbital with higher energy and the other bonding orbital with lower energy arising from the hybridization of two primitive plasmons known as "cavity plasmons" and "shell plasmons". However, experimental observations of plasmon hybridizations in the nanoshells are very few due to the limitation in the synthesis process. Although, few works on plasmon hybridization in nanoshells with solid dielectric core (silica) coated with a metal shell have been investigated [21, 25, 26], so far, there is no report in which the dielectric core is a gas. In this article, we have explored to investigate plasmon hybridization in silver nanoshells with a gaseous medium as a dielectric core. Nanoshells with varying diameters are synthesized in a

B. Mondal · S. K. Saha (✉)
Department of Materials Science, Indian Association for the Cultivation of Science, Jadavpur, Kolkata 700032, India
e-mail: cnssks@iacs.res.in

controllable way using hydrothermal process followed by calcinations. However, nanoshells with very small (<200 nm) and too large (>500 nm) diameters have not been achieved by this approach.

Experimental

To synthesize the silver nanoshells, in the first step; 1 g of Polyacrylamide (PAM) with Mw > 5,000,000 and PD ~ 1.302 obtained from BDH chemicals (Poole, England) is mixed with 200 mL of distilled water and stirred for nearly 15 min. The mixture is then kept for 1 week to get matured and used as stock solution. In the second step, 0.25 g silver nitrate (SN) purchased from Merck (Mumbai, India) is taken in a beaker with 10 mL of water and stirred well with a magnetic stirrer. 5 mL of stock solution is added to it while stirring. The mixture is transferred to a 70 mL homemade Teflon-lined steel autoclave and 80% of the autoclave is filled by adding 40 mL of distilled water. The mixture is heated for 2 h at different temperatures (T_H). The autoclave is brought out of the oven and cooled down to room temperature and the solution is stored in a beaker. A colloidal solution is obtained when the mixture is heated at 360 K and the color changes from yellow to red when it is heated to 415 K. At 510 K (T_H), a grayish precipitate is obtained. Twenty microliters (μL) of solution heated at 510 K (T_H) is spread in droplets by a micropipette on a silicon substrate to form uniform layer and calcinated at different temperatures (T_C) to form nanoshells.

Optical, morphological and microstructural characterizations of the final product have been carried out. The composites are collected from the hydrosol by filtration and dried at 330 K in a hot air oven. Crystalline phases of the samples have been characterized by a powder X-Ray Diffraction (XRD) using Rigaku diffractometer (Washington, USA). The decomposition temperature of PAM in the as-prepared sample is investigated by thermogravimetric analysis (TA Inst., Qsdt 600, USA). The solution heated at 415 K (T_H) was used to study the morphology and structures by a Scanning Electron Microscope (SEM, JEOL, JSM6700F, Tokyo, Japan). The hydrosol obtained after heating at different T_H is diluted properly and used to take absorption spectra with a Cary 5000 (Varian, Mumbai, India) spectrophotometer in transmission mode using water as reference. The silicon substrate after calcination is taken in a beaker with some water and sonicated for nearly 30 min to get a dark solution. The solution is used to record absorption spectra for nanoshells. Microstructures of nanoshells are studied using the carbon coated TEM grid with Transmission Electron Microscope (TEM, JEM-2010, Tokyo, Japan) having an electron diffraction apparatus at 200 kV.

Results and discussions

TGA analysis

Thermogravimetric Analysis (TGA) is performed to determine the decomposition temperature of PAM and PAM–silver composites. The TGA curve of PAM–silver composites shown in Fig. 1a has three regions where mass losses have been occurred. First one from 430 to 490 K (~15%) is due to adsorbed water on the surface and other volatile impurities [27], second one between 500 and 540 K (~9%) due to decomposition of residual amide groups and the third nearly 10% mass loss at 675 K is attributed to complete decomposition of PAM–silver composite. It may be noted from Fig. 1a that the decomposition temperature of PAM increases significantly due to formation of PAM–silver composite.

XRD studies

The XRD pattern reveals the overall crystal structure and phase purity of the as-synthesized samples. The XRD pattern of the PAM–silver composite (T_H ~ 510 K) is displayed in Fig. 1b (Graph-I). It shows that the composite is consisted of two phases, one is metallic silver indexed as (111), (200), (220), and (311) diffraction peaks of silver cubic structures with cell parameters, $a = 4.086$ (JCPDS file no. 04-0783) and the other one is non-crystalline PAM. The magnified image of the broad peak arising due to amorphous PAM present in the composites is shown in the inset. However, XRD of the silver nanoshells (Graph-II) obtained after calcination (T_H ~ 510 K and T_C ~ 650 K) of the PAM–silver composites shows no such broad region but the peaks become very sharp and intense due to increase in crystallinity. Moreover, presence of any other phases of silver or trace amount of SN is not found in the samples.

Growth mechanism of silver nanoshells

At temperature 360 K (T_H), PAM is hydrolyzed releasing ammonia (NH_3) gas [28], which in aqueous solution creates a reducing atmosphere as a result silver ions are reduced to form ultrafine silver NPs. These NPs are immediately attached to the PAM chains due to strong interaction of carbonyl group of PAM with NPs. Such type of interaction between PAM and silver NPs is also supported by XPS and FTIR studies [29]. At higher T_H (~415 K), the NPs along the PAM chain grow in size and form NPs assembly along PAM chain in the form of nanowires as shown in Fig. 2. When T_H is further increased to 510 K, the NPs assembly along with PAM chain is disrupted and the hydrosol is in thermal equilibrium with a

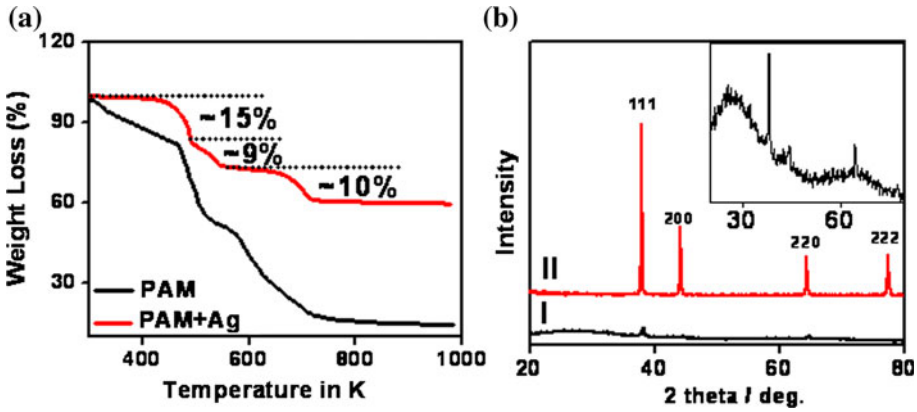

Fig. 1 **a** TGA of PAM and PAM–silver composites. **b** XRD of PAM–silver composites (*I*) before and (*II*) after calcinations. *Inset* is enlarged XRD pattern of the composites before calcinations to show the presence of amorphous PAM in it

homogeneous phase of NPs attached to disrupted PAM chains. These PAM–silver composites are agglomerated to form "globules" with dimension 300–400 nm as shown in Fig. 3a upon cooling to room temperature.

The electron beam of TEM was focused on a globule for long time during investigation of the microstructures. The portion under electron beam is burnt as shown in Fig. 3b and c due to the fact that long exposure time of electron beam produces large amount of heat, as a result, PAM is degraded to different gases (NH_3, CO_2, and water vapor) exposing the NPs as indicated by an arrow. HR-TEM image of the NPs in Fig. 3d shows the crystallographic planes of silver. Here, we like to emphasize that this composite is different from the conventional "nanocomposites" where only one phase (NPs) is in nanometric dimension while the other phase (matrix) is in the micro dimension. Therefore, the PAM–silver composite may be called as "nano-nanocomposite" as both phases are in the nanometric dimension. The composite globules obtained from hydrothermal process has no regular shape, however,

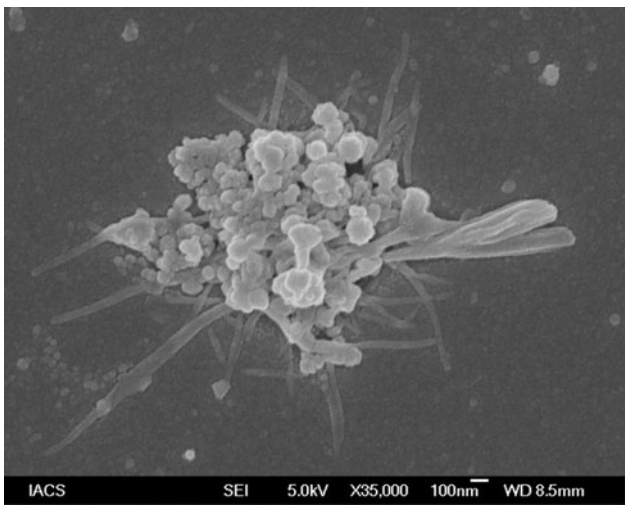

Fig. 2 FE-SEM image of assembly of silver nanoparticles along PAM chains. Some overgrowth of silver is also seen

during calcinations on the substrate at around 650 K (T_C), the softening temperature of PAM, the globule is in the molten state to form a highly viscous liquid like droplet of spherical shape to minimize the surface energy. This is the reason the globule shown in Fig. 4a to become spherical. As this T_C is very close to the degradation temperature of PAM and the fact that the decomposition temperature decreases abruptly in the nanophase, the fraction of PAM, remained in the composite is degraded to release gases from all parts of the globule. Released gases are trapped in the form of nanobubbles inside the molten globules. Large number of such trapped bubbles both on the surface as well as in the interior of the spherical globule is shown in Fig. 4a.

Formation of shell from the composite globules due to bubble formation in the interior of the globule is demonstrated in Scheme 1. The bubbles formed at different parts in the interior of the sphere were initially in the nanometric dimension and with time coalesced together to form a big bubble displacing the NPs radially outward. Due to nanometric dimension the buoyancy force on the bubble is not high enough to move in the upward direction. Similarly, nanobubbles formed on the outer surface of the globule coalesce to form a big bubble and trapped on the surface of the globule displacing the NPs radially inward. Under the action of these two opposite forces arising due to formation of big bubbles in the interior and on the surface of the globule, the NPs come very close to each other to form shells as shown in Fig. 4b and c. The inner and outer diameters of a nanoshell are approximately 232 and 370 nm, respectively, as indicated in Fig. 4d. From the high resolution TEM image of the boxed area of Fig. 4d, it is seen that the shell portion is composed of silver nanocrystals oriented in all possible directions as demonstrated in Fig. 4e. High resolution TEM reveals that major portion of the boxed area is consisted of nanocrystals with the resolved spacing of about 0.222 nm corresponding to the spacing of (111) lattice planes ($d = 0.228$ nm) of silver. The thick circular electron diffraction pattern taken from

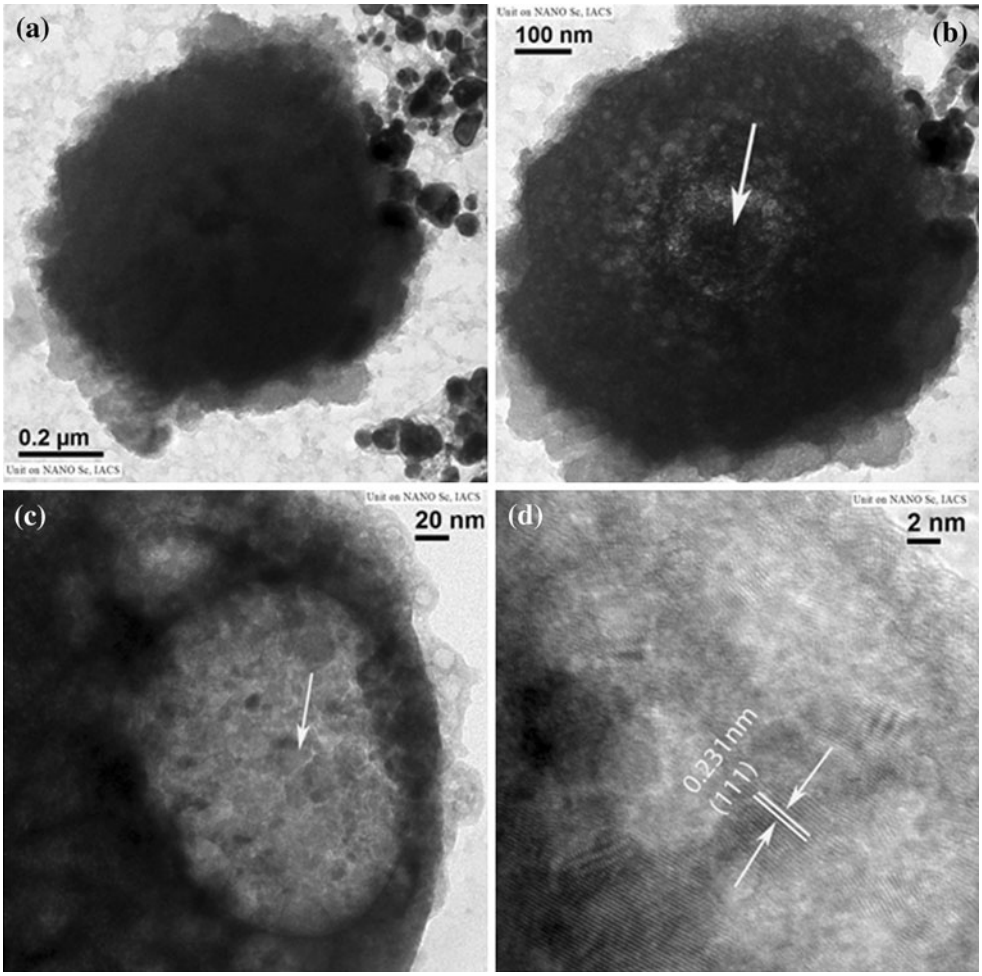

Fig. 3 **a** TEM image of PAM–silver composite globule. **b** and **c** Same globule after electron beam irradiation on it at two different positions. Silver NPs are seen at the beam-irradiated place **(d)**. HR-TEM image of **c** displays the crystallographic (111) plane of the silver NPs

the shell shown in the inset of Fig. 4a, also implies that the shell portion is composed of silver nanocrystals oriented in all possible directions. At moderate T_C ($\sim$650 K), when the gas cannot come out of the globule, the final shape of the composite particle looks like a spherical shell as shown in Fig. 4d. However, at sufficiently high T_C ($\sim$675 K), the gas pressure is so high that it comes out of the shell. During this process, the entire mass is in molten state and as a result the NPs are rearranged to form a torus like structure as shown in Fig. 4f. It may be mentioned that the thickness and outer diameters of the shells can be controlled by changing the PAM concentration. Different nanostructures obtained with variation in PAM, T_H, and T_C are summarized in Table 1.

UV–Vis spectra

Absorption spectra are a strong tool to investigate nanostructures by studying corresponding SPR which is very sharp for spherical mono dispersed NPs, and becomes broad for larger size NPs or heterogeneity in size and splits into two for nanoshells, one for lower energy (symmetric or bonding) SPR mode (ω_-) and the other for higher energy (anti-symmetric or anti-bonding) SPR mode (ω_+) due to hybridization. However, strength of interaction depends on the dimensions of the shell, for example in case of thin shell, bonding and anti-bonding modes are widely separated whereas, for thick shells the interaction is weak. Therefore, tuning of SPR modes as a result of hybridization depends not only on size of the nanoshells but also on the thickness of the shell.

Figure 5a shows the absorption spectra of the solution heated to different T_H. Absorption spectra of the hydrosol heated at 360 K show a single sharp peak due to isolated nanoparticle attached to PAM chains. When the hydrosol is heated at 380 K, more NPs are deposited along the PAM chains due to which plasmons of individual NPs start to interact and the absorption spectra become broad. The Lorentz de-convolution shows that the broad peak is consisted of two peaks, one at 441 nm and the other is at

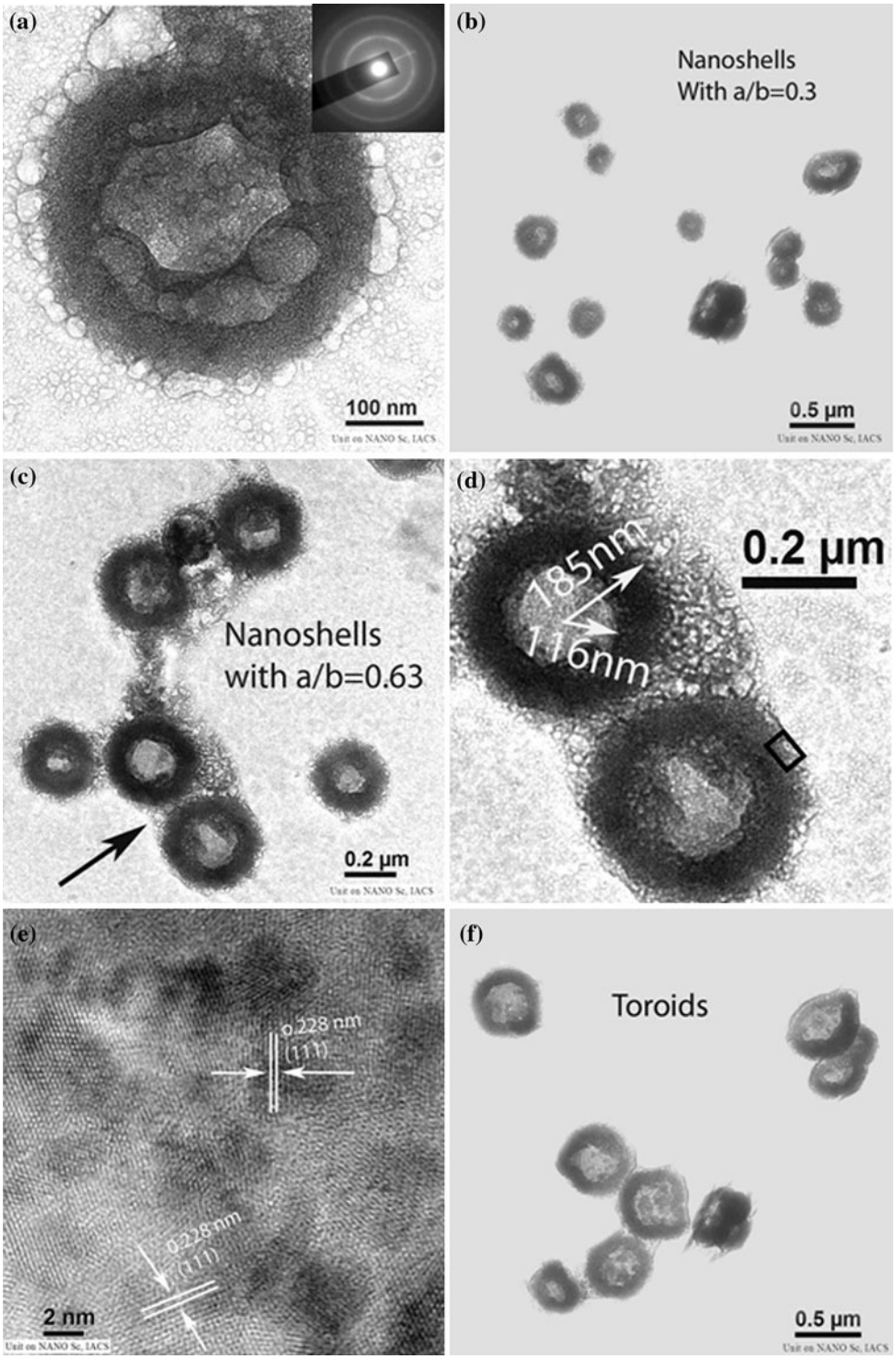

Fig. 4 **a** A shell with some bubbles around it with its SAED pattern in the *inset*. **b** The nanoshells obtained from composite globules after calcinations at 630 K. **c** Relatively bigger size nanoshells are obtained if the globules are calcinted at 650 K. **d** Approximate dimensions of a nanoshell. Outer and inner diameters of a nanoshell are calculated to be 370 and 232 nm, respectively. **e** HR-TEM of the *boxed area* of **d** shows that it is consisted of silver NPs of (111) planes. **f** Toroids obtained when the globules are calcinted at 675 K

524 nm due to hybridization between two primitive plasmons of NPs as shown in Fig. 5b. If the solution is heated to 415 K, the NPs along the PAM chain grow in size and form NPs assembly along PAM chain in the form of nanowires. The absorption spectra are characterized with two peaks one at 440 nm and the other very broad peak

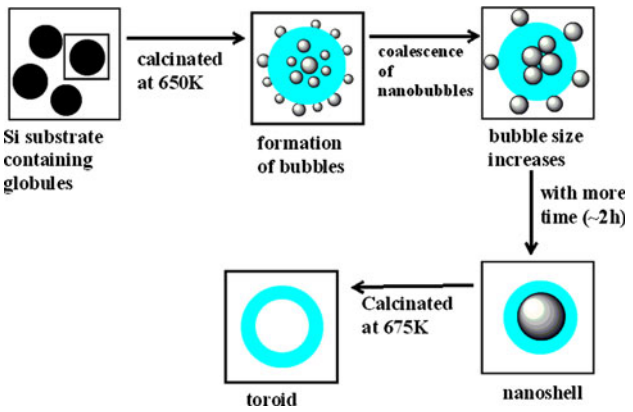

Scheme 1 Schematic of evolution of nanoshells and toroids from PAM–silver composite globules

between 660 and 1000 nm. The Lorentz de-convolution of the spectra shows two peaks one at 453 nm and the other at 949 nm, which are due to transverse and longitudinal SPR modes of nanowires, respectively as given in the inset of Fig. 5a. If the T_H is further increased to 510 K, there is only one broad peak. This is due to the fact that at this T_H the NPs assembly along with PAM chain is disrupted and the hydrosol is in thermal equilibrium with a homogeneous phase of NPs and disrupted PAM chains which forms globules upon cooling to room temperature.

The frequencies of the hybridized modes (bonding and anti-bonding) of SPR for small nanoshells in quasistatic limit can be expressed as [10],

$$\omega_{n\pm}^2 = \frac{\omega_B^2}{2}\left[1 \pm \frac{1}{2n+1}\sqrt{1+4n(n+1)\left(\frac{a}{b}\right)^{2n+1}}\right]$$

where "a" and "b" are the inner and outer radii of the shells, respectively, and 'n' is the order of spherical harmonics. Assuming, the bulk plasmon frequency of silver as 9.0×10^{14} Hz, the ratio of inner and outer radii (a/b) as 0.3, taken from Fig. 4b, the values of "ω_{n+}" and "ω_{n-}" have been calculated as 403 and 592 nm, respectively, which are very close to experimentally ($T_H = 510$ K and $T_C = 620$ K) observed values (407 and 584 nm, respectively) as demonstrated in Fig. 5c. However, Lorentz de-convoluted spectra show three peaks at 406, 572, and 660 nm. The first (406 nm) and the second (572 nm) peaks are very close to the theoretically calculated values of "ω_{n+}" and "ω_{n-}"of nanoshells. The origin of the third peaks is explained later. The absorption spectra for $T_H \sim 510$ K and $T_C \sim 650$ K have two SPR peaks at 447 nm and a broad peak centered at 654 nm. However, Lorentz de-convolution shows three SPR peaks at 431, 621, and 844 nm, respectively as shown in Fig. 5d. For thin walled nanoshells with a/b ratio 0.63 given in Fig. 4c, "ω_{n+}" and "ω_{n-}" have been calculated as 375 and 726 nm, respectively. To explain three Lorentz de-convoluted SPR peaks of the samples, we have considered the interaction between the shells. The nanoshells in the solution come very close to each other as also seen in Fig. 4c, and the SPR modes of individual nanoshells are further hybridized to form additional two peaks. The third peak in two spectra (660 nm for $a/b = 0.3$ and 844 nm for $a/b = 0.63$) is the bonding SPR mode (ω'_-) due to interaction between first and second peak (406 and 572 nm for $a/b = 0.3$; 431 and 621 nm for $a/b = 0.63$) and the peak arising for anti-bonding mode (ω'_+) of the first and the second will appear at around 320 nm. In the de-convoluted peaks, we do not find this peak as it is outside the measurement range; however, other three peaks are obtained at respective positions with very small deviations ($\sim$1 to 33 nm) from experimentally observed values. The deviations between the experimentally observed peak positions and that obtained from the de-convolution are attributed to the size inhomogeneity and mixed nature of the sample. Moreover, it may be mentioned that the positions of these two peaks depend on the distance between shells too.

Conclusion

Silver nanoshells with controlled diameters are synthesized by hydrothermal process just by changing T_H and T_C followed by calcinations on a silicon substrate. The growth mechanism and the plasmon hybridization of individual shell as well as the interaction of two shells with respect to

Table 1 Different nanostructures obtained with variation in T_H and T_C

Hydrothermal temperature (T_H) (K)	Calcinations temperature (T_C) (K)	Structures obtained
360	–	Silver nanoparticles
380	–	Cluster of silver nanoparticles
415	–	Assembly of nanoparticles along PAM
510	–	Globules
510	620	Small nanoshells
	650	Nanoshells
	675	Toroids

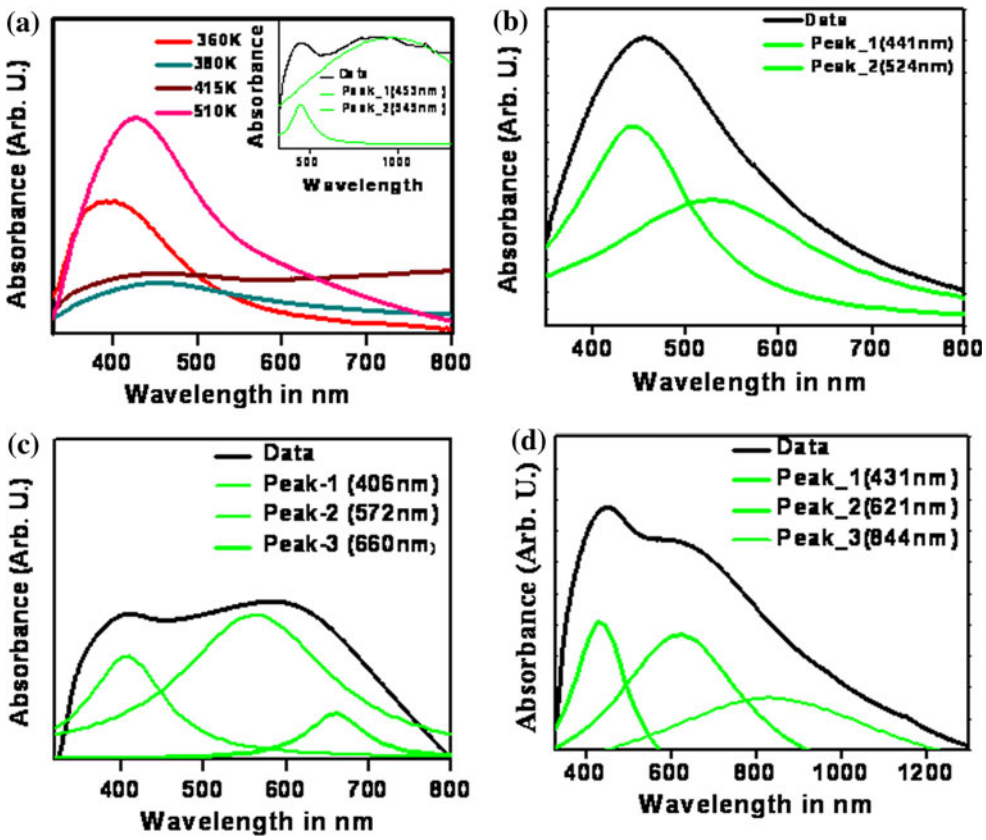

Fig. 5 **a** Absorption spectra of the solution for different T_H. *Inset* is spectra for the assembly of NPs with its Lorentz de-convolution. **b** Spectra of the hydrosol heated at 380 K and its Lorentz de-convolution. **c** The sample calcinted at 620 K shows two prominent peaks at 407 and 584 nm. **d** Absorption spectra for the sample calcinted at 650 K with its three Lorentz de-convolution

hybridization have been discussed. We believe that using this hydrothermal process with PAM as reducing agent, the nanoshells of other metals can be synthesized with controlled inner and outer radii just tuning the parameters T_H and T_C to use them in plasmonic devices.

Acknowledgements BM acknowledges CSIR, New Delhi, Govt. of India, for his fellowship and SKS acknowledges DST, New Delhi for financial support.

References

1. Wang H, Brandl DW, Norlander P, Halas NJ (2007) Acc Chem Res 40:53
2. Maier SA, Brongersma ML, Kik PG, Meltzer S, Requicha AG, Atwater HA (2001) Adv Mater 13:1501
3. Barnesl WL, Dereux A, Ebbesen TW (2003) Nature 24:824
4. Ozbay E (2006) Science 311:189
5. Atay A, Song JH, Nurmikko AV (2004) Nano Lett 4:1627
6. Koh AL, Bao K, Khan I, Smith WE, Kothleitner G, Nordlander P, Maier SA, McComb WD (2009) ACS Nano 3:3015
7. Gunnarsson L, Rindzevicius T, Prikulis J, Kasemo B, Zou MK, Schatz GC (2005) J Phys Chem B 109:1079
8. Prodan E, Nordlander P (2004) J Chem Phys 120:5444
9. Wang H, Wu Y, Lassiter B, Nehl CL, Hafner JH, Nordlander P, Halas NJ (2006) Proc Natl Acad Sci USA 103:10856
10. Funston A, Novo C, Davis TJ, Mulvaney P (2009) Nano Lett 9:1651
11. Willingham B, Brandl DW, Nordlander P (2008) Appl Phys B 93:209
12. Wang H, Brandl DW, Le F, Nordlander P, Halas NJ (2006) Nano Lett 6:827
13. Lassiter JB, Aizpurua J, Hernandez LI, Brandl DW, Romero I, Lal S, Hafner JH, Nordlander P, Halas NJ (2008) Nano Lett 8:1212
14. Prodan E, Radloff C, Halas NJ, Nordlander P (2003) Science 302:419
15. Prodan E, Nordlander N, Halas NJ (2003) Nano Lett 3:543
16. Prodan E, Nordlander P, Halas NJ (2003) Nano Lett 3:1411
17. Yang Y, Xiong L, Shi J, Nogami M (2006) Nanotechnology 17:2670
18. Chen C, Wang L, Li R, Jiang G, Yu H, Chen T (2007) J Mater Sci 42:3172. doi:10.1007/s10853-007-1594-x
19. Zhou L, Fu XF, Yu L, Zhang X, Yu XF, Hao ZH (2009) Appl Phys Lett 94:153102
20. Rycenga M, McLellan JM, Xia Y (2008) Adv Mater 20:2416
21. Jiang ZJ, Liu CY (2003) J Phys Chem B 107:12411
22. Germain V, Li J, Ingert D, Wang ZL, Pileni MP (2003) J Phys Chem B 107:8718
23. Nadagouda MN, Varma RS (2008) Cryst Growth Des 8:291
24. Lu X, Rycenga M, Skrabalak SE, Wiley B, Xia Y (2009) Annu Rev Phys Chem 60:167
25. Zhang J, Fu Y, Lakowicz JR (2007) J Phys Chem C 111:1955
26. Ling G, He J, Huang L (2004) J Mater Sci 39:2955. doi: 10.1023/B:JMSC.0000021490.52788.62
27. Chen M, Wang LY, Han JT, Zhang JY, Li ZY (2006) J Phys Chem B 110:11224
28. Caulfield MJ, Qiao GG, Solomon DH (2002) Chem Rev 102:3067
29. Mukherjee S, Mukherjee M (2006) J Phys Condens Matter 18:11233